NEAR-ULTRAVIOLET AND NEAR-INFRARED SPACE-WEATHERING TRENDS AT MARE AND HIGHLAND SWIRLS. David T. Blewett[1,*], Brett W. Denevi[1], Joshua T. S. Cahill[1], and Rachel L. Klima[1]. [1]Planetary Exploration Group, Johns Hopkins University Applied Physics Laboratory, Laurel, MD 20723, USA (*david.blewett@jhuapl.edu).

Introduction: Solar-wind ion bombardment is one of the agents responsible for altering the optical properties of materials that are exposed on the surfaces of airless bodies. Micrometeoroid impacts are also thought to play an important role in such optical alteration, which is termed "space weathering" [e.g., 1, 2], although the relative contribution to space weathering by the solar wind and micrometeoroids is not fully understood and can vary from place to place in the Solar System [e.g., 3] and on the Moon [4, 5]. Typical lunar space weathering involves introduction of a strong positive ("red") spectral slope from the visible to near-infrared (NIR), an overall decrease in reflectance, and weakening of Fe^{2+} absorption bands near 1000 and 2000 nm. The effects of lunar-style space weathering in the ultraviolet (UV) were described by Hendrix and Vilas [6]. The near-UV (NUV) slope at wavelengths shortward of 415 nm is steep in fresh material and shallows (becomes "bluer") in more mature material [6, 7]. The optical alteration is caused by the accumulation of submicroscopic blebs and coatings of iron (SMFe) on and within regolith particles [1, 8]. These NIR and NUV effects are illustrated in Fig. 1, using laboratory spectra for lunar soils and crushed lunar rocks (from RELAB and also Wagner et al. [9]). We plot the NIR ratio (1550-nm/700-nm, a measure of continuum slope) vs. the NUV ratio (321-nm/415-nm). Fig. 1 shows that soils have steep (red) NIR continua and shallow (blue) NUV ratios. The reverse is true of the rocks, which have shallow NIR continua but steep NUV slopes. However, the low-Fe highland samples (black triangles) show little variation in the NUV ratio as a function of maturity [7].

Lunar Swirls and Anomalous Weathering: Areas of magnetized crustal rocks (magnetic anomalies) have been mapped globally by *Lunar Prospector* [e.g., 10, 11], and magnetic anomalies are known to decrease the flux of solar-wind ions reaching the lunar surface [e.g., 12–14]. Hence, it might be expected that a magnetically shielded area could experience atypical space weathering [15]. Indeed, the unusual high-albedo markings called lunar swirls [e.g., 16–20] are all collocated with magnetic anomalies.

We have undertaken an analysis of spectral trends in order to gain further insight into the nature and origin of swirls and the causes of lunar space weathering.

Spacecraft Observations: Prior studies have examined lunar swirls with data from the *Clementine* UVVis camera [e.g., 4, 18, 19, 21–23], the *Clementine* NIR camera [19], M^3 [24–26], *Kaguya* Multiband Imager (MI) [23], and in the far-UV using LAMP [27, 28]. LROC NUV images have proven to be especially useful for mapping swirls [7, 20].

We perform an analysis similar to that of Hemingway et al. [4], who defined regions of interest (ROIs) on and around the high-reflectance portions of mare swirls in *Clementine* images in order to characterize the behavior in terms of the 950-nm/750-nm reflectance ratio and 750-nm reflectance. Those workers found that the swirl maturity trajectory in this spectral space differs from the trend in non-swirl surfaces. We use the NIR continuum ratio (1550-nm/700-nm, from topographically corrected *Kaguya* MI [25]) to focus on the effects of SMFe on continuum slope. This ratio is favored over the 950-nm/750-nm ratio, which is a function of both the continuum slope and the strength of the 1000-nm band. We simultaneously examine swirls in the NUV using LROC WAC [26].

Results: Figs. 2 and 3 demonstrate that separate normal and anomalous (swirl) trends are evident in the NUV and NIR for the Reiner Gamma (RG) swirl. Bright swirl pixels lie along trends that are shallower than that of the mature background, attesting to unusual optical alteration within the swirl. The swirl pixels also have higher NIR and NUV ratios than predicted for normal (fresh) material of the same albedo.

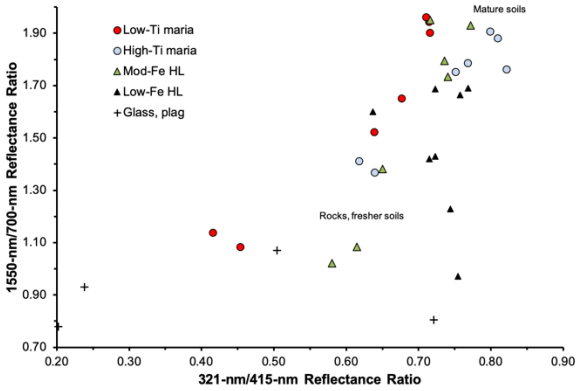

Fig. 1. NIR ratio vs. NUV ratio, for spectra of lunar soils and powdered lunar rocks. Higher NIR ratio = steeper NIR continuum. Higher NUV ratio = shallower NUV slope.

Similar to RG, the Airy highland swirl has a weathering trend in the NIR that differs from the nearby background (Fig. 4). Airy swirl materials have NUV ratio

values that are similar to or slightly lower than the mature background (Fig. 5). This is consistent with the subdued NUV variation with maturity seen in highland samples (Fig. 1) and in LROC NUV images of the highlands [7].

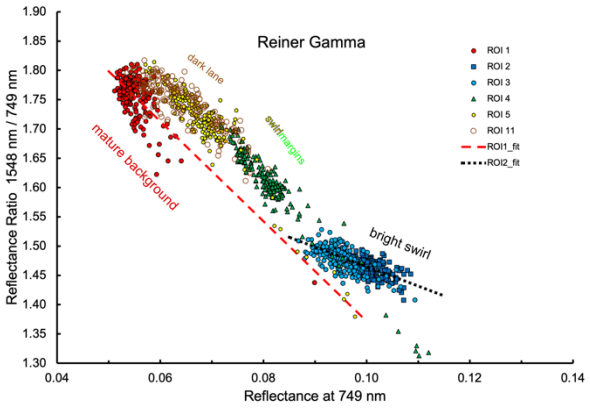

Fig. 2. NIR ratio vs. 749-nm reflectance for Reiner Gamma swirl ROI pixels. Dashed line fits indicate weathering trends within background and swirl material.

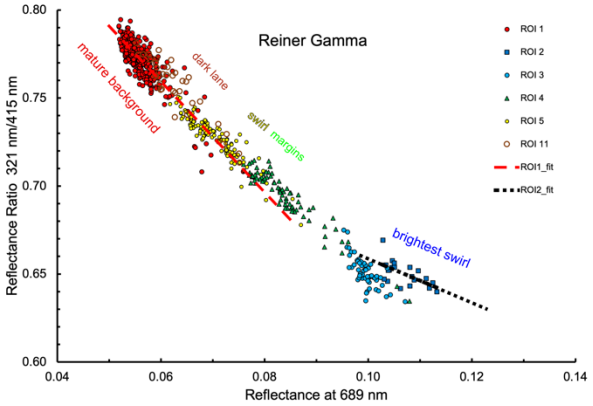

Fig. 3. NUV ratio vs. 689-nm reflectance for RG ROIs.

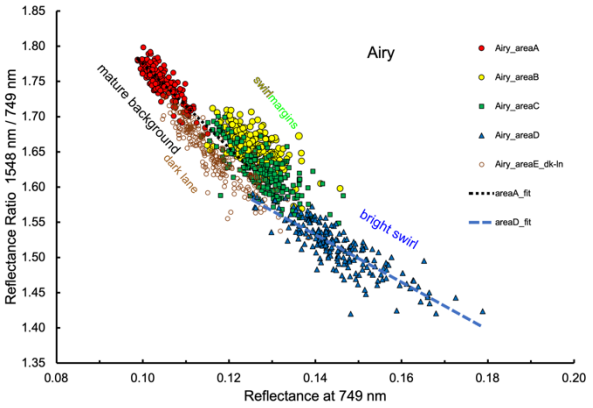

Fig. 4. NIR ratio vs. 749-nm reflectance for Airy ROIs.

We have performed similar analyses for four additional swirls. Our work builds on that of Hemingway et al. [4] by extending the study to both mare and highland swirls and by considering spectral behavior in both the NIR and in the NUV. Observations include the following. The bright portions of mare swirls have NIR ratios that are lower than the mature background (lower NIR continuum), and NUV ratios that are lower than the mature background (steeper NUV slopes). The bright portions of highland swirls have NIR ratios that are lower than the mature background (lower NIR continuum), and NUV ratios that are similar to or slightly lower than that of the mature background. We are interpreting these spectral characteristics in terms of the size distribution of SMFe [27, 28].

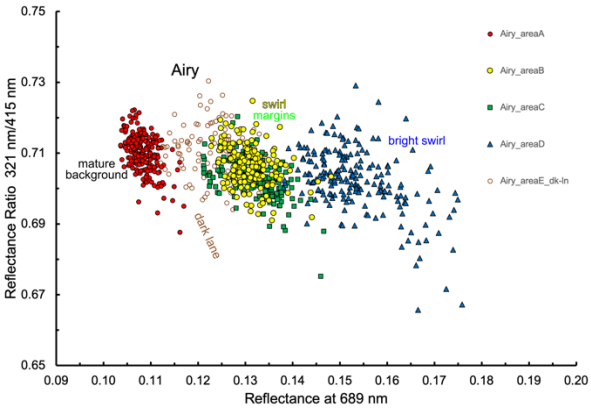

Fig. 5. NUV ratio vs. 689-nm reflectance for Airy ROIs.

References: [1] B. Hapke (2001), *JGR 106*, 10,039. [2] C. Pieters and S. Noble (2016), *JGRP 121*. [3] D. Domingue et al. (2014), *SSR 181*, 121. [4] D. Hemingway et al. (2015), *Icarus 261*, 66. [5] C. K. Sim et al. (2017), *GRL 44*. [6] A. Hendrix and F. Vilas (2006), *Astron. J. 132*, 1396. [7] B. Denevi et al. (2014), *JGRP 119*. [8] C. Pieters et al. (2000), *MPS 35*, 1101. [9] J. Wagner et al. (1987), *Icarus 69*, 14. [10] L. Hood et al. (2001), *JGR 106*, 27,825. [11] J. Halekas et al. (2001), *JGR 106*, 27,841. [12] M. Kurata et al. (2005), *GRL 32*, L24205. [13] J. Halekas et al. (2008), *PSS 56*, 941. [14] M. Weiser et al. (2010), *GRL 37*, L05103. [15] L. Hood and G. Schubert (1980), *Science 208*, 49. [16] P. Schultz and L. Srnka (1980), *Nature 284*, 22. [17] L. Hood and C. Williams (1989), *Proc. LPSC 19th*, 99. [18] D. Blewett et al. (2011), *JGR 116*, E02002. [19] G. Kramer et al. (2011), *JGR 116*, E04008. [20] B. Denevi et al. (2016), *Icarus 273*, 53. [21] P. Pinet et al. (2000), *JGR 105*, 9457. [22] I. Garrick-Bethell et al. (2011), *Icarus 212*, 480. [23] J. McFadden et al. (2019), *Icarus 333*, 323. [24] G. Kramer et al. (2011), *JGR 116*, E00G18. [25] C. Pieters et al. (2014), *LPSC 45*, abstr. 1408. [26] K. Chrbolková et al. (2019), *Icarus 333*, 516. [27] A. Hendrix et al. (2016), *Icarus 273*, 68. [28] J. Cahill et al. (2019), *JGRP 124*. [25] M. Lemelin et al. (2015), *JGRP 120*. [26] A. Boyd et al. (2012), *LPSC 43*, abstr. 2795. [27] S. Noble et al. (2007), *Icarus 192*, 629. [28] D. Trang and P. Lucey (2019), *Icarus 321*, 307.